ARTICLE TYPE www. rsc.org/xxxxxx | XXXXXXXX

To access the final edited and published work see http://dx.doi.org/10.1039/C1SC00676B

A TD-DFT study of the effects of structural variations on the photochemistry of polyene dyes

Saurabh Agrawal, Pratibha Dev, Niall J. English,* K. Ravindranathan Thampi* and J. M. D. MacElroy

Received Xth XXXXXXXXXX 20XX, Accepted Xth XXXXXXXXX 20XX

First published on the web Xth XXXXXXXXXX 200X

DOI: 10.1039/b000000x

We report a TD-DFT study of three polyene dyes namely: NKX-2553, NKX-2554 and NKX-2569 in isolation as well as upon their adsorption on TiO_2 nanoparticles. By choosing closely related dyes we wish to focus on the effects of structural variations on the absorption and charge-transfer properties of these systems. These three dyes show a non-intuitive trend in their respective efficiencies and therefore, were chosen to shed light on the structural components that contribute to this behaviour. Although, NKX-2554 has an additional donor group, it is less efficient compared to the simpler NKX-2553 dye that contains only one donor group. When NKX-2554 structure is slightly modified by lengthening the linker-group, one obtains the most efficient dye among this set, namely, NKX-2569. In this work, we show that the changes in the donor moiety has very little or no effect on the efficiency of these dyes as can be seen in the case of NKX-2553 and NKX-2554. On the other hand, the improved performance of NKX-2569-titania complex can be understood to be a result of the longer linker group. A better understanding of these properties within different dye-titania complexes is important for the continual improvement of DSSCs. In this regards, this study will serve to provide guidelines to improve efficiencies of novel organic dyes.

1 Introduction

World-wide concern towards green house gases has generated immense research interest in alternative energy sources like solar cells. Solar cells being used to-date are mostly silicon-based. Although silicon based cells are efficient, they are expensive due to highly purified solar-grade silicon that is required for their fabrication. On the other hand, dye sensitized solar cells (DSSCs) can be made more affordable due to the use of cheaper semiconductors like TiO_2. Due to this, DSSCs have become an active area of research since they were first introduced.[1] A typical DSSC consists of a layer of dye molecules adsorbed on semiconductor electrode surface, a consecutive layer of electrolyte (I/I_3^-) and a counter electrode deposited with Pt or carbon particles. In these cells, current generation takes place by photooxidation of the dye. The excited dye transfers its charge into the conduction band of semiconductor that lies at a lower energy level compared to the excited state of the dye. The oxidized dye is reduced back to its original state by I/I_3^- electrolyte. The cycle is completed as the charge is transferred across the external circuit to the counter electrode.[2] Although, this mechanism seems straight forward, it involves high level of complexities. A recent review by Hagfeldt *et al*[3] provides a brief description of the intricacies involved in the process.

The overall efficiency of a DSSC critically depends on the dye(s) employed as photo-sensitizers in the cell. As a result, novel dyes with better efficiencies and stability are being investigated. So far, the state-of-the-art ruthenium-based sensitizers give the conversion efficiencies exceeding 11%.[4–6] Although efficient, Ru-based dyes are not cost effective. Therefore, to reduce the manufacturing cost of the DSSCs various metal-free, organic dyes are now being proposed and investigated. These organic dyes are advantageous due to their adjustable spectral and the electrochemical properties.[7,8]

A typical organic sensitizer consists of a donor group (electron donating group), a linker group and an acceptor/anchor moiety (electron accepting group). An appreciable number of organic dyes have been reported with different types of donors, linkers and acceptors. Among the donor moieties, *N*,*N*-dimethylaniline group,[9,10] coumarins,[11–17] tetrahydroquinolines,[18,19] pyrrolidine,[20] carbazoles,[21] diphenylamine,[22] triphenylamine,[23–26] etc have been widely used for the dye synthesis. A linker moiety is a spacer added between the donor and acceptor moieties. Different π-conjugated linker groups such as the —C=C— chain,[9–13,16,24] thiophene units (and its derivatives),[11,14–22,26] etc have also been investigated. In particular two types of acceptor/anchor groups, namely cyanoacrylic acid,[9–26] and carboxylic acid[27–29] are widely used in organic dyes for DSSC.

The SFI SRC in Solar Energy Conversion, School of Chemical and Bioprocess Engineering, University College Dublin, Belfield, Dublin 4, Ireland; Tel: +353 1 716 1646; E-mail: niall.english@ucd.ie (N. J. English); Tel: +353 1 716 1995; Email: ravindranathan.thampi@ucd.ie (K. R. Thampi)

Charge injection/transfer (CT) from dye to the conduction band of the semiconductor is one of the key processes that is important for DSSC's performance. CT rate depends on several features of the conjugated structure. The efficiency of the injection process depends on the electronic coupling between the dye and the metal-oxide surface. Asbury *et al*[30] found that the time for electron injection increases with the reduction of electronic coupling between the dye and the semiconductor. The rate of charge injection also depends on the electronic character of the conduction band of the semiconductor. For example, the conduction band of TiO_2 is derived mostly from the *3d*-orbitals of titanium atoms. This high density of empty states in TiO_2 results in a fast CT rate.[30,31]

Upon excitation, the injection of the charge from the dye to the semiconductor can occur through either of the two mechanisms – direct and indirect. In the direct mechanism, under optimal conditions of electronic coupling between the dye and the semiconductor, CT takes place in one step from ground state of the dye to the conduction band of the semiconductor. On the other hand, in case of indirect mechanism, the process is completed in two steps: (1) the charge is excited from the ground state of the dye to another state that is localized on dye itself and (2) the charge then tunnels from the excited dye into the conduction band of the semiconductor.[32,33] In direct CT, a new band may appear in the absorption spectrum of the complex which is not present in the spectra of the isolated dye and surface individually. The origin of a new absorption peak suggests a strong electronic interaction between the dye and the semiconductor.[34] Although, a new peak gives indication of direct CT, it is not present in all direct-mechanism cases that have been studied to-date. Some of the theoretical studies observed the presence of a new band[31,35] while others did not find new peaks although the charge injection was attributed to the direct transfer mechanism.[36–38]

As detailed above, many factors decide the efficiency of dye-titania complexes. In this work, we have systematically studied the effects of donor and linker moieties on the dye's performance. To do so, we have studied three closely related polyene dyes. These dyes were introduced by Hara and coworkers[9,10]. They all have *N*,*N*-dimethylaniline (DMA) donor which is used due to its simple structure and strong electron-donating ability. Among this class of dyes, NKX-2553, NKX-2554 and NKX-2569 (Figure 1) have demonstrated 5.5%, 5.4% and 6.8% efficiencies respectively under AM 1.5 irradiation. Here, the NKX-2553 dye has one DMA as donor whereas, NKX-2554 and NKX-2569 have two DMA donor groups. In these dyes, the donor is connected to different π-conjugated linker moieties, which are further attached with cyanoacrylic acid. Both, NKX-2553 and NKX-2554 have a three carbon atom linker chain with alternative single and double bonds as shown in Figure 1. Compared to these dyes, NKX-2569 has a longer linker moiety with a total of five carbon atoms (Figure 1c). All three dyes have cyanoacrylic acid as the acceptor/anchor group. The NKX-2553, NKX-2554 and NKX-2569 show open circuit voltages (V_{oc}) of 0.71 V, 0.74 V and 0.71 V and short-circuit photocurrent densities (J_{sc}) of 10.4, 9.9 and 12.9 mA cm^{-2}, respectively. Fill factor for all of these devices is 0.74.[9]

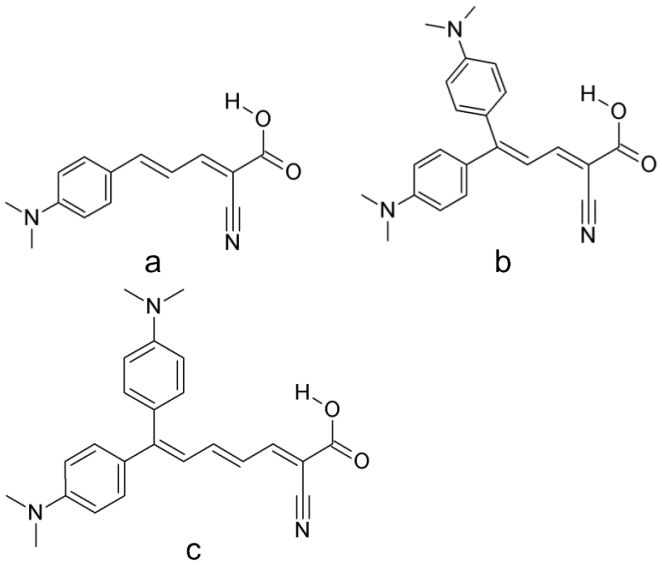

Figure 1 Schematic diagram of (a) NKX-2553, (b) NKX-2554 and (c) NKX-2569 dyes.

As compared to NKX-2553, NKX-2554 shows slight reduction in efficiency and J_{sc} values in spite of an extra donor group. On the other hand, NKX-2569 that also contains two DMA units, performs best with 6.8% efficiency. The key to better performance of NKX-2569 as compared to the other two dyes seem to lie in its longer linker chain leading to the better charge separation between donor and linker moieties. Understanding the structural properties and their relation with the dye performance is very important for designing better dyes that yield more efficient DSSCs. Therefore, in this theoretical study, we have investigated the possible effects of donor and linker moieties on the photoexcitation and charge transfer properties of organic dyes when they are chemisorbed on TiO_2 nanoparticles.

2 Computational details

NKX-2553, NKX-2554 and NKX-2569 dyes were modeled using Discovery Studio Visualizer package (Accelrys, San Diego, CA). In the first step of the calculations, we carried out ground state structural optimization of the isolated dyes, using B3LYP hybrid functional and 6-31G* basis sets. The effects of the solvent (acetonitrile) were added using the polarizable

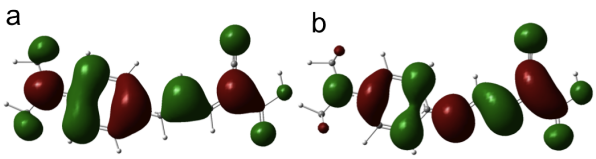

Figure 2 MOs of NKX-2553 dye involved in photoexcitation. (a) HOMO and (b) LUMO

continuum model of solvation (C-PCM)[39] as implemented in the Gaussian 09 software suit.[40] Geometry optimizations were followed by single point TD-DFT calculations to obtain the UV/VIS spectra of the three dyes. The next step in this work was to optimize the dye-titania structures. To do so, we prepared a neutral, stoichiometric cluster of $(TiO_2)_{38}$ exposing the anatase 101 surface, as described by Persson et al[41]. Previous studies[37,38,42] have shown that the lowest excitation energy of the $(TiO_2)_{38}$ cluster is in good agreement with the experimental bandgap of a nanoparticle of a few nanometer size. As the conjugated structures were very large and computationally demanding, we used the plane-wave DFT code Quantum Espresso (4.2.1)[43] to obtain reasonable geometries for the dye-titania complexes. These calculations were done using generalized gradient approximation (GGA) of Perdew-Burke-Ernzerhof (PBE) to account for the exchange-correlation effects.[44] As we used ultrasoft (US) pseudopotentials, we found that an energy cutoff of 50 Ry gives converged results. The atomic relaxations were carried out until the residual forces were less than 10^{-3} Ry/au. Each dye-titania complex was separated from its images by addition of vacuum layers ($\geq$9 Å-thick) in the x-, y- and z- directions. Optimization of geometry was followed by single point TD-DFT calculations using a Gaussian 09 software suit. The basis set and the exchange-correlation functions were identical to those used for the isolated dyes.

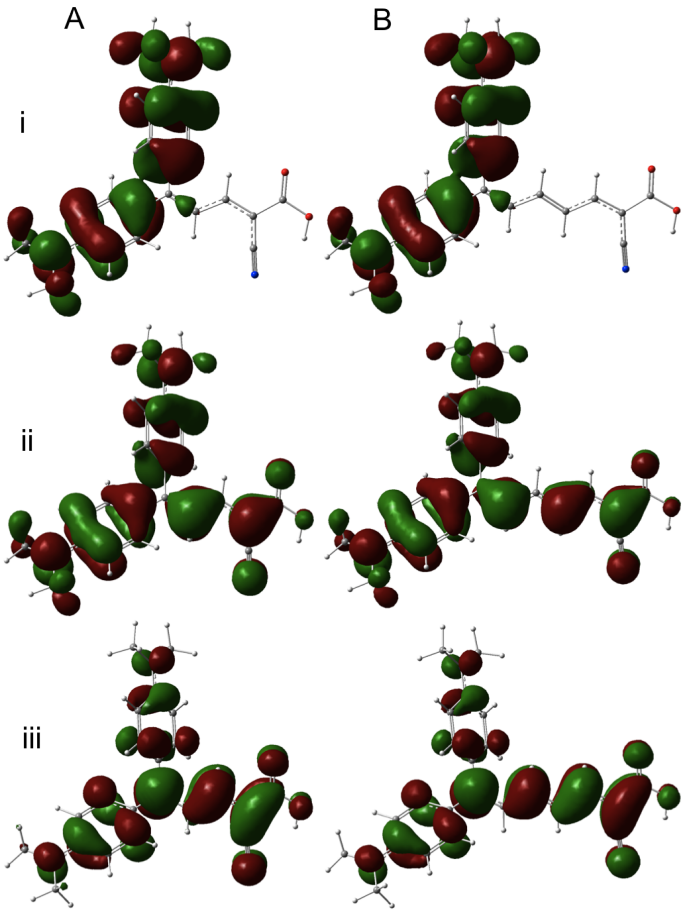

Figure 3 MOs involved in photoexcitation for (A) NKX-2554 and (B) NKX-2569 dyes. Here, (i) HOMO-1, (ii) HOMO and (iii) LUMO

3 Results and discussion

3.1 Electronic structure and absorption spectra of dyes

Optimized geometries and frontier orbitals (isovalue 0.02 e/a.u^3) for NKX-2553, NKX-2554 and NKX-2569 are given in Figure 2, Figure 3(A) and Figure 3(B), respectively. For all the three dyes, the highest occupied molecular orbital (HOMO) and lowest unoccupied molecular orbital (LUMO) show π- and π^*-character, respectively. In all the three cases, HOMOs are delocalized over the almost entire molecule with a slightly more localization on DMA donor moieties compared to the cyanoacrylic acid (acceptor/anchor) group. LUMOs also show delocalization over the entire dye molecules with a little more localization on the acceptor as compared to the donor. This localization of HOMO over donor groups and

Table 1 Theoretically calculated λ_{max} and their corresponding HOMO (H), LUMO (L) energies and H-L gap (Δ_{HL}) in eV units

Molecules	λ_{max}	H	L	Δ_{HL}
NKX-2553	2.74	-5.34	-2.52	2.82
NKX-2554	2.61	-5.23	-2.45	2.78
NKX-2569	2.26	-5.05	-2.62	2.43
TiO_2	3.65	-7.70	-3.24	4.46
NKX-2553/TiO_2	2.24	-5.41	-3.17	2.24
NKX-2554/TiO_2	2.20	-5.37	-3.14	2.23
NKX-2569/TiO_2	1.82	-5.11	-3.15	1.96

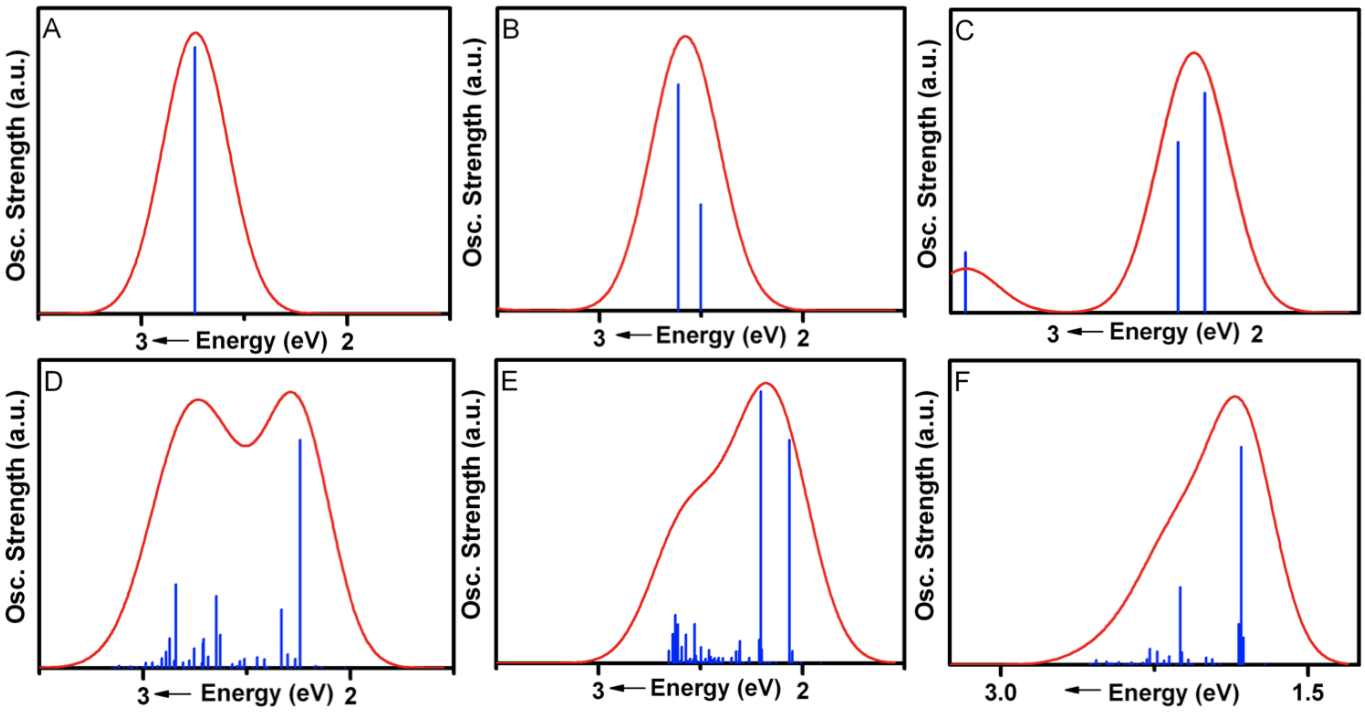

Figure 4 UV/Vis absorption spectra of (A) NKX-2553, (B) NKX-2554, (C) NKX-2569, (D) NKX-2553/TiO_2, (E) NKX-2554/TiO_2 and (F) NKX-2569/TiO_2.

Table 2 Transitions corresponding to λ_{max} and other major peaks for dyes.

Dyes Excitation State:	T. E. (eV) (O.S. (f))	Wave function (Coefficients)
NKX-2553		
1:	2.74 (1.40)	**H→L (0.71)**
NKX-2554		
1:	2.50 (0.42)	H-1→L (0.60), H→L (0.38)
2:	2.61 (0.90)	H-1→L (-0.38), **H→L (0.60)**
NKX-2569		
1:	2.26 (0.94)	H-1→L (0.29), **H→L (0.65)**
2:	2.39 (0.73)	H-1→L (0.64), H→L (-0.29)
3:	3.42 (0.26)	H-2→L (0.67), H→L (-0.20)

T.E. is Transitional Energy and O.S. is Oscillator strength.

localization of LUMO over acceptor/anchor groups is desirable for the charge separation, which leads to the push-pull effect.

The experimental UV/Vis absorption spectra[9] show maximum absorbances (λ_{max}) for NKX-2553 at 2.71 eV, NKX-2554 at 2.68 eV and NKX-2569 at 2.47 eV. Our calculated absorption spectra show λ_{max} at 2.74 eV for NKX-2553 (Figure 4A), 2.61 eV for NKX-2554 (Figure 4B) and at 2.26 eV for NKX-2569 dyes (Figure 4C and Table 1). Apart from the excitation peak at λ_{max}, NKX-2554 and NKX-2569 also show additional excitations at 2.50 eV and 2.39 eV, respectively (Table 2). These excitations increase absorption ranges for NKX-2554 and NKX-2569 dyes. In the case of these two dyes, not only HOMO but also HOMO-1 shows its contribution in excitation at λ_{max} (Table 2). Further, HOMO-1 is mostly localized on donor moieties as shown in Figure 3(A)(i) and 3(B)(ii). These results show that the addition of an extra donor moiety, assists NKX-2554 and NKX-2569 to achieve slight red-shift and broadening of the absorption peaks compared to NKX-2553. Additionally, in the case of NKX-2569, increase in the length of linker moiety further shifts the absorption peak towards the red part of the spectrum. These red-shifts in absorption spectra are attributed to the increase in the π-conjugation of NKX-2554 and NKX-2569 dyes. This broadening and red shift in the spectra was also observed in

the experimental data[9]. Overall, the two shorter dyes – NKX-2553 and NKX-2554 – show better agreement with experimental results as compared to NKX-2569. The latter one shows a slight underestimation of excitation energy at λ_{max} and gives a red-shift of ∼0.21 eV compared to the experimental value. This can be understood as an inadequacy of the the exchange-correlation functionals to properly describe the excitations involving charge-transfer. The conventional functionals like GGA and LDA do not contain the correct 1/R-dependence (R is the charge separation distance) and so fail to correctly predict the energies for charge transfer transitions. The hybrid functionals such as B3LYP and PBE0 partially alleviate this problem by the inclusion of the exact exchange interaction. Although B3LYP is an improvement over the conventional functionals, it is still not perfect with its $0.2\,R^{-1}$ dependence instead of R^{-1}. As a result, the excitation energies for the charge transfer interactions are underestimated within B3LYP. This error increases with increasing distance between the charge donor and charge acceptor as is the case of NKX-2569. [45]

HOMO and LUMO energies as well as, the HOMO-LUMO gap (Δ_{HL}) are given in Table 1. Here, NKX-2553 shows HOMO at -5.34 eV, LUMO at -2.52 eV and Δ_{HL} 2.82 eV. The Δ_{HL} value reduces to 2.78 eV for NKX-2554 with the placement of HOMO (-5.23 eV) and LUMO (-2.45 eV) at higher energies compared to the respective MOs of NKX-2553. Among these dyes, NKX-2569 shows the lowest Δ_{HL} of 2.43 eV with the HOMO and LUMO states at -5.05 eV and -2.62 eV energies respectively. These results (Table 1) show that the Δ_{HL} value follows the order, NKX-2569 < NKX-2554 < NKX-2553. This decrease in Δ_{HL} is attributed to the increased π-conjugation in the larger dyes. Table 1 also gives the valence band maximum and conduction band minimum of the titania nanoparticle. The placement of HOMO and LUMO of the dyes relative to the bandgap of titania is an important factor for their performance as a sensitizer. Ideally, HOMO of the dye should be situated within the bandgap of TiO_2. Here, the HOMOs for all the three dyes are placed within the Δ_{HL} of TiO_2 and LUMO is situated at an energy higher than the conduction band minimum of the isolated TiO_2 (Table 1). The calculated absorption spectra of the isolated TiO_2 lies mostly in UV-range and starts at ∼3.6 eV. This is in a good agreement with the experimental band gap of titania nanoparticles that are a few nanometers in size. [46]

The dipole moments for NKX-2553, NKX-2554 and NKX-2569 are 16.22, 16.24 and 19.98 D, respectively. The larger dipole moment of NKX-2569 gives it the desirable greater charge separation upon excitation. On the other hand, NKX-2553, NKX-2554 have comparable dipole moments that might explain the similar efficiencies shown by the two dyes, even though, the latter has an additional DMA donor in its structure.

3.2 Electronic structure and absorption spectrum of dye/TiO_2 complexes

So far, we have described how the structural properties of the dyes might affect their electronic structure. The relative positions of the dye's HOMO and LUMO levels within the titania band structure affect the overall efficiency of the DSSC. It is not sufficient to look at the electronic structures of these systems individually. So, the next step in this research was to look at the dye/titania complexes. On TiO_2, surface chemisorption of the dye takes place through acidic dissociation of the carboxylic acid anchor. In this, hydrogen atom dissociates from the carboxylic acid and bond formation takes place between carboxylate oxygen atoms and the surface titanium atoms of the metal oxide. An FTIR study by Hara and coworkers [16] showed that the coumarin based NKX-2311 dye containing cyanoacrylic acid anchor is adsorbed on TiO_2 in a bidentate carboxylate mode. Another study by the same group also shows that one more cyanoacrylic acid anchor based NKX-2553 dye is adsorbed on TiO_2 in bidentate carboxylate mode as well. [10] Furthermore, FTIR study by Srinivas *et al* [47] on cyanoacrylic acid adsorption on TiO_2 rules out possibility of physisorption, and authors suggest cyanoacrylic acid adsorption through bidentate bridging mode. On the basis of these studies, we have used bidentate bridging mode for dye adsorption on TiO_2 nanoparticle.

The optimized geometries of NKX-2553/TiO_2, NKX-2554/TiO_2 and NKX-2569/TiO_2 complexes are given in Figure 5, Figure 6(A) and Figure 6(B), respectively. The bond distances between two carboxylate oxygens and the titanium atoms on the surface are: (1) 2.01 Å and 2.03 Å for NKX-2553/TiO_2, (2) 2.00 Å and 1.98 Å for NKX-2554/TiO_2, and (3) 1.99 Å and 2.01 Å for NKX-2569/TiO_2 complex. The bond distances and angles for dye-titania complexes at the interface are provided in Figure 7.

3.3 NKX-2553/TiO_2 complex

Although experimental absorption spectra for these dye-surface complexes are not yet available, IPCE (Incident-Photon-to-electron Conversion Efficiency) spectra give considerable insight into light absorption trend of the systems. Therefore, we compare our absorption spectra of the dye-surface complexes with the respective IPCE spectra. The experimental IPCE spectrum [9] for NKX-2553/TiO_2 complex begins from ∼1.63 eV and shows more than 70% IPCE between ∼ 2.07 eV to ∼ 2.7 eV. Theoretically calculated absorption spectra for NKX-2553/TiO_2 complex shows absorption band onsets from ∼ 1.70 eV (FWHM used is 0.37 eV) with λ_{max} at 2.24 eV(Figure 4D), which is in agreement with the experimental results. The calculated absorption peak at λ_{max} shows red-shift of ∼ 0.5 eV compared to the λ_{max} of the isolated dye. The absorption spectra for the complex consists of

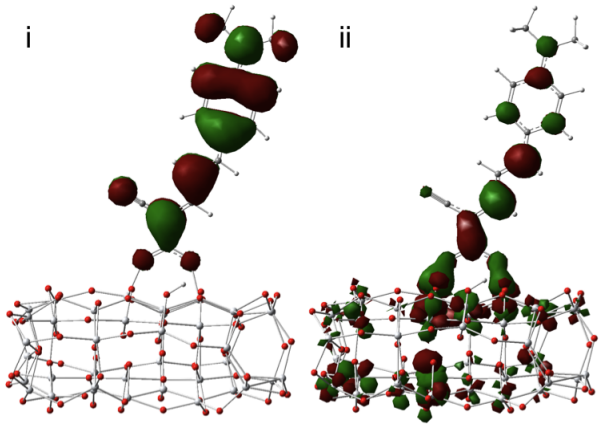

Figure 5 MOs of NKX-2553/TiO_2 complexes involved in photoexcitation. Here, (i) HOMO and (ii) LUMO+3

many photo-excitations. Some of these excitations showing high oscillator strengths with their contributing molecular orbitals (MOs) are given in Table 3. HOMO participates in all of the high intensity excitations and is localized on dye part of the complex as can be seen from Figure 5(i) (isovalue 0.02 e/a.u^3). HOMO of the complex is characteristically similar to HOMO of the isolated dye.

The unoccupied orbitals that participate in major photo-excitations can be seen to range from LUMO+3 to LUMO+35 (Table 3). The excitation taking place at λ_{max} involves LUMO+3 and LUMO+4. Among these orbitals, LUMO+3 has maximum contribution (Table 3) and is shown in Figure 5(ii). The isosurface plot for LUMO+3 shows that it is delocalized on both the dyes as well as on the nanoparticle. This in turn shows a strong hybridization between the titania and dye states. Due to considerable delocalization of LUMO+3 on anchor moiety of dye as well as on the titania nanoparticle, one can envisage a direct charge transfer mechanism for NKX-2553 dye. Furthermore, the strong hybridization between the states of the two sub-systems manifests itself in the new photo-excitation peak that appear in the spectrum and which was absent in the spectra of two isolated sub systems of the complex. The presence of the new excitations further supports direct charge transfer for the complex.

3.4 NKX-2554/TiO_2 complex

IPCE for NKX-2554/TiO_2 complex also starts from ∼1.63 eV and shows more than 70% IPCE between ∼2.07 eV to ∼2.7 eV.[9] In agreement with the experiment, the theoretical absorption spectrum for the complex shows absorbance from ∼1.65 eV with maximum absorbance peak at 2.20 eV (Figure 4E). As compared to the isolated NKX-2554 dye, dye-titania complex exhibits ∼0.4 eV red-shift at λ_{max}. Absorption band for the

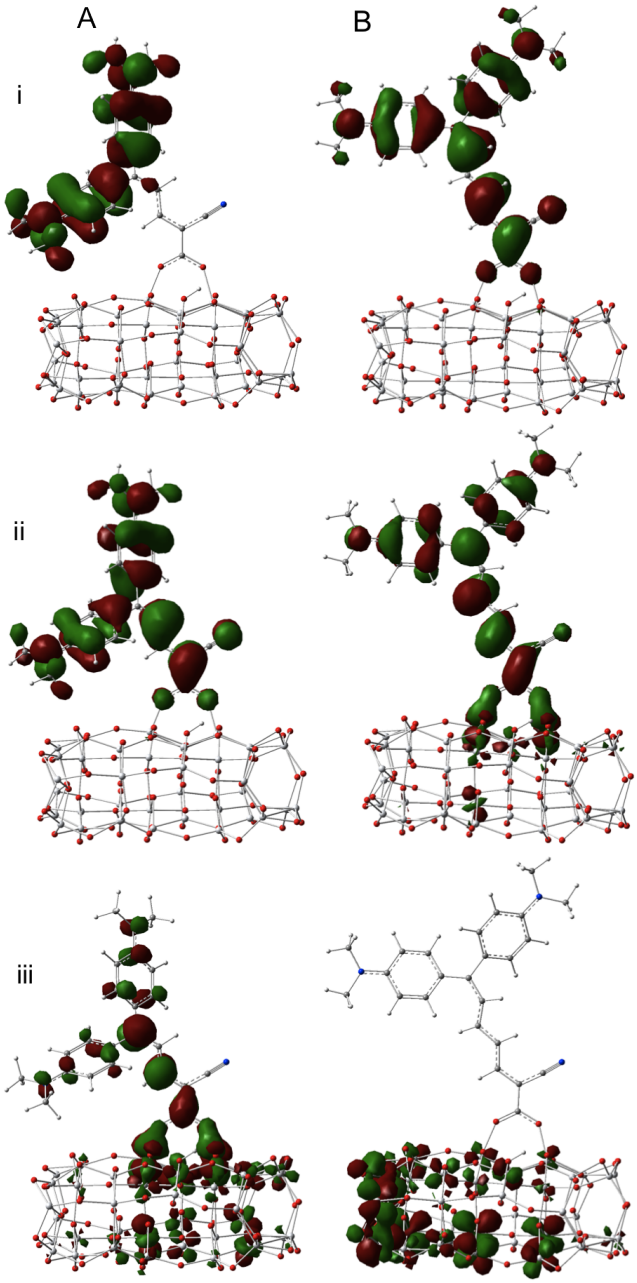

Figure 6 (A) MOs involved in the photoexcitation of NKX-2554/TiO_2 complex. The isosurface plots are given for (i) HOMO-1, (ii) HOMO and (iii) LUMO+3. (B) MOs involved in the photoexcitation of NKX-2569/TiO_2 complex. The isosurface plots are given for (i) HOMO, (ii) LUMO+1 and (iii) LUMO+2

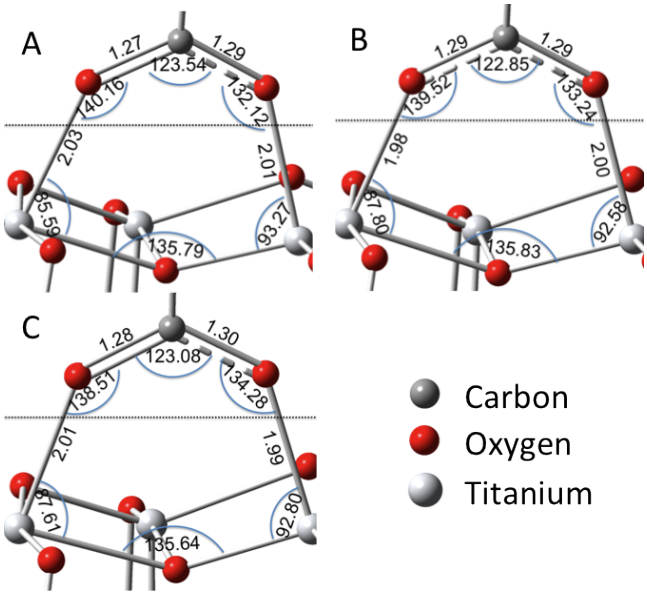

Figure 7 Structural details for dye-titania complexes at the interface. The horizontal dotted line in the figure is drawn to demarcate the interface between the dye and the surface. (A) NKX-2553/TiO_2, (B) NKX-2554/TiO_2 and (C) NKX-2569/TiO_2.

complex also shows a new shoulder between ∼2.4 eV - ∼2.7 eV, which is absent in the isolated dye. Here, several photo-excitations are involved in the formation of total absorption spectrum. A few of these excitations having relatively high oscillator strengths are given in Table 3 conjointly with their corresponding MOs. Most of these photo-excitations originate from HOMO-1 and HOMO (Figure 8, column 5). Isosurfaces plotted for both HOMO-1 (Figure 6(A)(i)) and HOMO (Figure 6(A)(ii)) of the complex show resemblance with HOMO-1(Figure 3(A)(i)) and HOMO (Figure 3(A)(ii)) of the isolated dye respectively. As shown in Figure 6(A), HOMO-1 is localized on DMA donor whereas HOMO is localized on entire dye part of the complex. Apart from HOMO-1 and HOMO, orbitals from HOMO-2 to HOMO-4 also shows dye character (Figure 8, column 4). These occupied states lie within HOMO-LUMO gap of isolated TiO_2 nanoparticle.

The unoccupied orbitals involved in the major excitations come from LUMO+3 to LUMO+26 (Table 3). Among these unoccupied orbitals, LUMO+3 shows highest contribution to the λ_{max} as well as to the second highest intensity peak at 2.06 eV. The isosurface plot for LUMO+3 (Figure 6(A)(iii)) shows that it is localized mostly on the linker and anchor moieties of the dye as well as on the surface atoms. The unoccupied orbitals below LUMO+3 are localized on surface with no contribution from the dye (Figure 8, col. 5). The delocalization of LUMO+3 on the dye as well as on the surface and presence of a new absorption peaks for complex suggests direct charge transfer from NKX-2554 to TiO_2 nanoparticle.

3.5 NKX-2569/TiO_2 complex

The theoretical absorption spectrum for NKX-2569/TiO_2 begins from ∼1.4 eV (Figure 4F), which is close to the origin of IPCE from ∼1.51 eV onwards.[9] When compared to NKX-2553 and NKX-2554, NKX-2569 shows ∼10% IPCE loss from ∼2.07 eV to ∼3.2 eV absorption energy and ∼20% gain towards higher wavelength light (from ∼1.55 eV to ∼1.72 eV). Theoretical absorption spectra shows a maximum absorbance at 1.82 eV, which is considerably red-shifted compared to NKX-2553 (λ_{max} = 2.24 eV) and NKX-2554 (λ_{max} = 2.06 eV) dye-surface complexes. The MOs involved in two high intensity excitations at 1.83 eV and 2.12 eV are given in Table 3. HOMO-1 is around 0.32 eV below the energy level of HOMO and participates in the lower wavelength excitation at 2.12 eV. On visualization, HOMO-1 of the complex is similar to HOMO-1 of the isolated dye (figure is not given). Additionally, HOMO contributes in both major excitations and is localized over the entire dye similar to the HOMO of the isolated dye (Figure 6(B)(i)).

Among the unoccupied orbitals LUMO+1, LUMO+2 and LUMO+11 are involved in the photo-excitations. Here, LUMO+1 shows highest contribution and is present in both the excitations. The isosurface for LUMO+1 (Figure 6(B)(ii)) is localized mostly on the dye and to some extent, on the titanium atoms attached to it. In contrast, LUMO+2 is localized only on nanoparticle with no contribution from the dye (Figure 6(B)(iii)). LUMO of this complex is also localized only on surface as indicated in Figure 8. The localization of LUMO+1 mostly on dye suggests indirect charge transfer mechanism. Here, upon excitation, the charge goes from the highest occupied level which is localized mostly on the dye to a higher state (LUMO+1) which is again localized on the dye and then tunnels to the nanoparticle. On the other hand, the involvement of LUMO+2 suggests a direct charge transfer due to its localization on the surface. Although, both direct as well as indirect charge transfer mechanisms might come into play for NKX-2569/TiO_2 complex, indirect mechanism seems to be the prominent mechanism for charge transfer as this happens with a higher probability as indicated by the (un-normalized) single CI coefficient of 0.56 compared to 0.39 for the other transition.

Amongst the studied complexes, NKX-2569/TiO_2 has the lowest Δ_{HL}, which allows the lower energy photons to participate in charge-transfer. This is supported by the λ_{max} as well as the comparatively higher IPCE at the longer wavelengths[9]. Furthermore, NKX-2553/TiO_2 and NKX-2554/TiO_2 complexes show direct charge transfer upon excitation. In contrast, in case of NKX-2569/TiO_2 complex, both direct as well as indirect charge-transfer mechanisms may play a role in the in-

Table 3 Transitions corresponding to λ_{max} and other major peaks for the dye/TiO_2 complexes

Complexes Excitation State:	Transition energy (eV) (Oscillator strength (f))	Wave function (Coefficients)
NKX-2553/TiO_2		
1:	2.24 (0.59)	**H→L+3 (0.67)**, H→L+4 (-0.15)
2:	2.33 (0.15)	H→L+5 (0.20), H→L+6 (-0.11), H→L+7 (0.64), H→L+10 (0.10)
3:	2.65 (0.19)	H→L+19 (0.10), H→L+20 (0.41), H→L+21 (-0.38), H→L+22 (0.34), H→L+26 (-0.15)
4:	2.84 (0.22)	H→L+31 (-0.12), H→L+32 (0.62), H→L+33 (0.23), H→L+35 (-0.11)
NKX-2554/TiO_2		
1:	2.06 (0.33)	H-1→L+3 (0.24), H→L+1 (-0.11), H→L+3 (0.61), H→L+4 (-0.12)
2:	2.20 (0.40)	**H-1→L+3 (0.61)**, H-1→L+4 (-0.11), H→L+3 (-0.23), H→L+6 (0.11), H→L+7 (0.14)
3:	2.62 (0.07)	H-1→L+19 (0.15), H-1→L+20 (0.36), H-1→L+26 (0.16), H→L+20 (-0.18), H→L+21 (0.18), H→L+25 (0.13), H→L+26 (0.39)
NKX-2569/TiO_2		
1:	1.83 (1.00)	**H→L+1 (0.56)**, H→L+2 (0.39)
2:	2.12 (0.36)	H-1→L+1 (0.67), H→L+11 (-0.18)

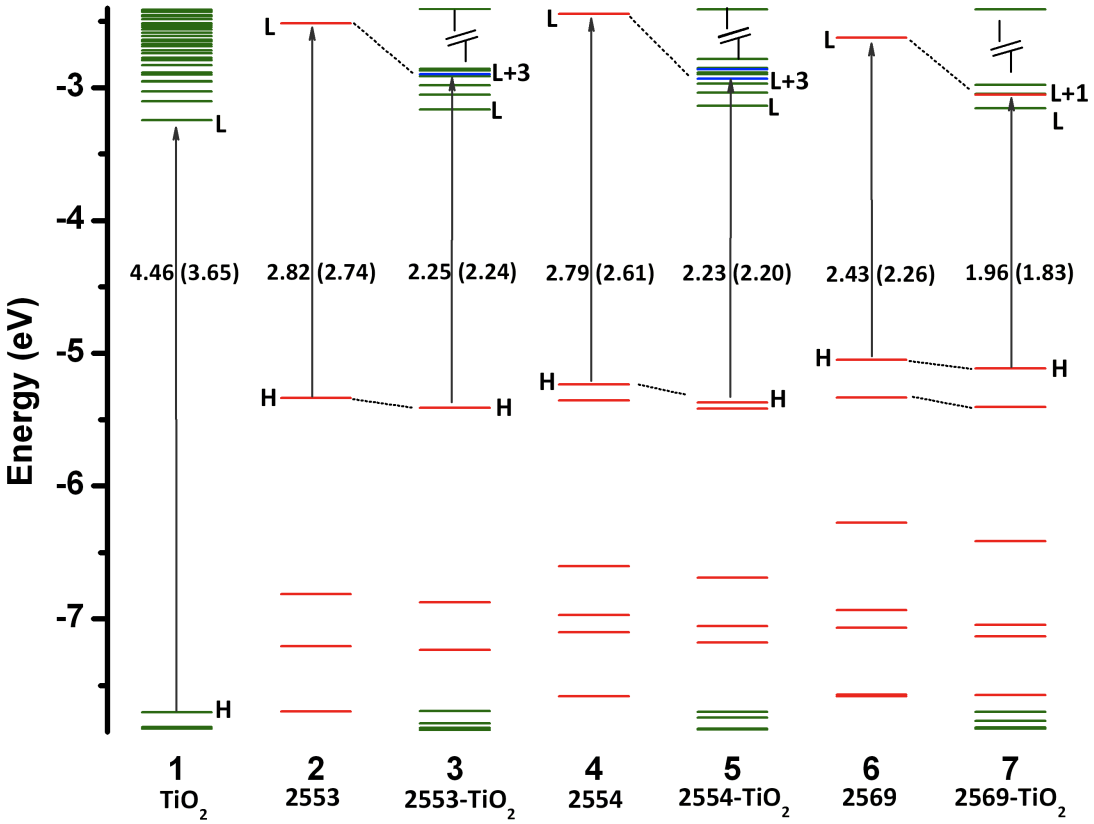

Figure 8 Molecular orbital energy level diagram of (column 1) isolated $(TiO_2)_{38}$ nanoparticle, (column 2) NKX-2553 dye, (column 3) NKX-2553/TiO_2 complex, (column 4) NKX-2554 dye, (column 5) NKX-2554/TiO_2 complex, (column 6) NKX-2569 dye and (column 7) NKX-2569/TiO_2 complex. Here, red represents localization of MO on the dye, green represents localization of MOs on the nanoparticle and blue represents localization of MOs both on the dye and the surface. Values given in small brackets refer to the TD-DFT excitation energies.

jection of the charge into titania. The charge-transfer through both mechanism provides NKX-2569 an additional edge over the two other dyes studied in this work. This might be the reason for its better efficiency than NKX-2553 and NKX-2554 dyes. This study shows that the extended π-conjugation at linker part for these dyes has higher impact on the enhancement of efficiency than the donor part. Apart from these polyene dyes many other dyes [12,13] have shown increase in the efficiency with increase in linker length. Although extended length increases the dye efficiency it also leads to the instability of the molecule. In this regard, this study will be useful towards the development of a predictive method to understand this phenomenon *a priori*.

3.6 Conclusion

This work presents detailed TD-DFT calculations for three polyene dyes in isolation as well as in conjugation with anatase (101) TiO_2 nanoparticle. The increase in the length of π-conjugated linker in NKX-2569 dye will lead to a better charge separation between the donor and acceptor moieties. This eventually should contribute in the reduction of charge recombination upon photoexcitation. Moreover, among the dye/titania complexes, NKX-2569/TiO_2 complex shows λ_{max} at lowest energy. The red-shift of the absorbance maximum of dye/TiO_2 complexes compared to the dyes, suggests better stabilization of the molecular orbitals due to hybridization of the dye and the nanoparticle states. Furthermore, on the basis of our results, we predict the direct charge-transfer mechanism for adsorbed NKX-2553 and NKX-2554 dyes. On the other hand, results for NKX-2569/TiO_2 complex indicate that both direct as well as indirect charge-transfer mechanisms might play a role, thereby, enhancing its performance over the other two structurally-related dyes. The latter conclusion is corroborated by the experimental results.

4 Acknowledgements

This material is based upon work supported by the Science Foundation Ireland (SFI) under Grant No. [07/SRC/B1160]. Dr P. Dev acknowledges financial support from the Irish Research Council for Science and Engineering (IRCSET).

References

1 B. O'Regan and M. Grätzel, *Nature*, 1991, **353**, 737–740.
2 M. Grätzel, *J Photochem. Photobio. C: Photochem. Reviews*, 2003, **4**, 145.
3 A. Hagfeldt, G. Boschloo, L. Sun, L. Kloo and H. Pettersson, *Chemical Reviews*, 2010, **110**, 6595–6663.
4 M. Grätzel, *Journal of Photochemistry and Photobiology A: Chemistry*, 2004, **164**, 3–14.
5 M. K. Nazeeruddin, F. De Angelis, S. Fantacci, A. Selloni, G. Viscardi, P. Liska, S. Ito, B. Takeru and M. Grätzel, *J Am Chem Soc*, 2005, **127**, 16835–47.
6 M. K. Nazeeruddin, A. Kay, I. Rodicio, R. Humphrybaker, E. Muller, P. Liska, N. Vlachopoulos and M. Grätzel, *J Am Chem Soc*, 1993, **115**, 6382–6390.
7 A. Mishra, M. K. Fischer and P. Bauerle, *Angew Chem Int Ed Engl*, 2009, **48**, 2474–99.
8 H. Tian and F. Meng, *Organic Photovoltaics: Mechanisms, Materials, and Devices*, Eds.: S.-S. Sun, N. S. Sariciftci, CRC, London,, 2005.
9 K. Hara, M. Kurashige, S. Ito, A. Shinpo, S. Suga, K. Sayama and H. Arakawa, *Chemical Communications*, 2003, 252–3.
10 K. Hara, T. Sato, R. Katoh, A. Furube, T. Yoshihara, M. Murai, M. Kurashige, S. Ito, A. Shinpo, S. Suga and H. Arakawa, *Advanced Functional Materials*, 2005, **15**, 246–252.
11 K. Hara, M. Kurashige, Y. Dan-oh, C. Kasada, A. Shinpo, S. Suga, K. Sayama and H. Arakawa, *New Journal of Chemistry*, 2003, **27**, 783–785.
12 K. Hara, K. Sayama, Y. Ohga, A. Shinpo, S. Suga and H. Arakawa, *Chemical Communications*, 2001, 569–570.
13 K. Hara, Y. Tachibana, Y. Ohga, A. Shinpo, S. Suga, K. Sayama, H. Sugihara and H. Arakawa, *Solar Energy Materials and Solar Cells*, 2003, **77**, 89–103.
14 K. Hara, Z. S. Wang, T. Sato, A. Furube, R. Katoh, H. Sugihara, Y. Dan-Oh, C. Kasada, A. Shinpo and S. Suga, *J Phys Chem B*, 2005, **109**, 15476–82.
15 K. Hara, K. Miyamoto, Y. Abe and M. Yanagida, *J Phys Chem B*, 2005, **109**, 23776–8.
16 K. Hara, T. Sato, R. Katoh, A. Furube, Y. Ohga, A. Shinpo, S. Suga, K. Sayama, H. Sugihara and H. Arakawa, *J. Phys. Chem. B*, 2003, **107**, 597–606.
17 Z.-S. Wang, Y. Cui, Y. Dan-oh, C. Kasada, A. Shinpo and K. Hara, *The Journal of Physical Chemistry C*, 2007, **111**, 7224–7230.
18 R. K. Chen, X. C. Yang, H. N. Tian and L. C. Sun, *Journal of Photochemistry and Photobiology a-Chemistry*, 2007, **189**, 295–300.
19 R. K. Chen, X. C. Yang, H. N. Tian, X. N. Wang, A. Hagfeldt and L. C. Sun, *Chemistry of Materials*, 2007, **19**, 4007–4015.
20 P. Qin, X. Yang, R. Chen, L. Sun, T. Marinado, T. Edvinsson, G. Boschloo and A. Hagfeldt, *The Journal of Physical Chemistry C*, 2007, **111**, 1853–1860.
21 Z.-S. Wang, N. Koumura, Y. Cui, M. Takahashi, H. Sekiguchi, A. Mori, T. Kubo, A. Furube and K. Hara, *Chemistry of Materials*, 2008, **20**, 3993–4003.
22 K. Thomas, J. Lin, Y. Hsu and K. Ho, *Chemical Communications*, 2005, 4098–4100.
23 S. Hwang, J. H. Lee, C. Park, H. Lee, C. Kim, C. Park, M.-H. Lee, W. Lee, J. Park, K. Kim, N.-G. Park and C. Kim, *Chem. Commun.*, 2007, 4887–4889.
24 W. Xu, B. Peng, J. Chen, M. Liang and F. Cai, *Journal of Physical Chemistry C*, 2008, **112**, 874–880.
25 W. H. Liu, I. C. Wu, C. H. Lai, P. T. Chou, Y. T. Li, C. L. Chen, Y. Y. Hsu and Y. Chi, *Chemical Communications*, 2008, 5152–4.
26 D. P. Hagberg, T. Marinado, K. M. Karlsson, K. Nonomura, P. Qin, G. Boschloo, T. Brinck, A. Hagfeldt and L. Sun, *J Org Chem*, 2007, **72**, 9550–6.
27 S. Tan, J. Zhai, H. Fang, T. Jiu, J. Ge, Y. Li, L. Jiang and D. Zhu, *Chem. Euro. J.*, 2005, **11**, 6272–6.
28 K. Tanaka, K. Takimiya, T. Otsubo, K. Kawabuchi, S. Kajihara and Y. Harima, *Chemistry Letters*, 2006, **35**, 592–593.
29 J.-H. Yum, P. Walter, S. Huber, D. Rentsch, T. Geiger, F. Nüesch, F. De Angelis, M. Grätzel and M. K. Nazeeruddin, *Journal of the American Chemical Society*, 2007, **129**, 10320–10321.
30 J. B. Asbury, E. Hao, Y. Wang, H. N. Ghosh and T. Lian, *The Journal of*

Physical Chemistry B, 2001, **105**, 4545–4557.
31 W. R. Duncan and O. V. Prezhdo, *The Journal of Physical Chemistry B*, 2005, **109**, 365–373.
32 D. Rocca, R. Gebauer, F. De Angelis, M. K. Nazeeruddin and S. Baroni, *Chemical Physics Letters*, 2009, **475**, 49–53.
33 R. Sánchez-de-Armas, J. Oviedo, M. A. San-Miguel, J. F. Sanz, P. Ordejón and M. Pruneda, *Journal of Chemical Theory and Computation*, 2010, **6**, 2856–2865.
34 W. R. Duncan and O. V. Prezhdo, *Annual Review of Physical Chemistry*, 2007, **58**, 143–184.
35 R. Sánchez-de-Armas, J. Oviedo, M. A. San Miguel and J. F. Sanz, *The Journal of Physical Chemistry C*, 2011, **115**, 11293–11301.
36 F. De Angelis, S. Fantacci, E. Mosconi, M. K. Nazeeruddin and M. Grätzel, *The Journal of Physical Chemistry C*, 2011, **115**, 8825–8831.
37 F. De Angelis, *Chemical Physics Letters*, 2010, **493**, 323–327.
38 S. Agrawal, P. Dev, N. J. English, K. R. Thampi and J. M. D. MacElroy, *Journal of Materials Chemistry*, 2011, **21**, 11101.
39 M. Cossi, N. Rega, G. Scalmani and V. Barone, *Journal of Computational Chemistry*, 2003, **24**, 669–681.
40 M. J. Frisch, G. W. Trucks, H. B. Schlegel, G. E. Scuseria, M. A. Robb, J. R. Cheeseman, G. Scalmani, V. Barone, B. Mennucci, G. A. Petersson, H. Nakatsuji, M. Caricato, X. Li, H. P. Hratchian, A. F. Izmaylov, J. Bloino, G. Zheng, J. L. Sonnenberg, M. Hada, M. Ehara, K. Toyota, R. Fukuda, J. Hasegawa, M. Ishida, T. Nakajima, Y. Honda, O. Kitao, H. Nakai, T. Vreven, J. A. Montgomery, Jr., J. E. Peralta, F. Ogliaro, M. Bearpark, J. J. Heyd, E. Brothers, K. N. Kudin, V. N. Staroverov, R. Kobayashi, J. Normand, K. Raghavachari, A. Rendell, J. C. Burant, S. S. Iyengar, J. Tomasi, M. Cossi, N. Rega, J. M. Millam, M. Klene, J. E. Knox, J. B. Cross, V. Bakken, C. Adamo, J. Jaramillo, R. Gomperts, R. E. Stratmann, O. Yazyev, A. J. Austin, R. Cammi, C. Pomelli, J. W. Ochterski, R. L. Martin, K. Morokuma, V. G. Zakrzewski, G. A. Voth, P. Salvador, J. J. Dannenberg, S. Dapprich, A. D. Daniels, O. Farkas, J. B. Foresman, J. V. Ortiz, J. Cioslowski and D. J. Fox, *Gaussian 09 Revision A.1*, Gaussian Inc. Wallingford CT 2009.
41 P. Persson, R. Bergstrom and S. Lunell, *The Journal of Physical Chemistry B*, 2000, **104**, 10348–10351.
42 F. De Angelis, A. Tilocca and A. Selloni, *Journal of the American Chemical Society*, 2004, **126**, 15024–15025.
43 P. Giannozzi, S. Baroni, N. Bonini, M. Calandra, R. Car, C. Cavazzoni, D. Ceresoli, G. L. Chiarotti, m. Cococcioni, I. Dabo, A. D. Corso, S. Fabris, G. Fratesi, S. de Gironcoli, R. Gebauer, U. Gerstmann, C. Gougoussis, A. Kokalj, M. Lazzeri, L. Martin-Samos, N. Marzari, F. Mauri, R. Mazzarello, S. Paolini, A. Pasquarello, L. Paulatto, C. Sbraccia, S. Scandolo, G. Sclauzero, A. P. Seitsonen, A. Smogunov, P. Umari and R. M. Wentzcovitch, *0906.2569*, 2009.
44 J. P. Perdew, K. Burke and M. Ernzerhof, *Physical Review Letters*, 1996, **77**, 3865–3868.
45 A. Dreuw and M. Head-Gordon, *Chemical Reviews*, 2005, **105**, 4009–4037.
46 Y.-X. Weng, Y.-Q. Wang, J. B. Asbury, H. N. Ghosh and T. Lian, *The Journal of Physical Chemistry B*, 1999, **104**, 93–104.
47 K. Srinivas, K. Yesudas, K. Bhanuprakash, V. J. Rao and L. Giribabu, *Journal of Physical Chemistry C*, 2009, **113**, 20117–20126.